



Best estimate plus uncertainty analysis of metal-water reaction transient experiment

Alan Matias Avelar^{a,*}, Camila Diniz^a, Fábio de Camargo^b, Claudia Giovedi^c, Alfredo Abe^c, Marco Cherubini^d, Alessandro Petruzzi^d, Marcelo Breda Mourão^a

^a Department of Metallurgical and Materials Engineering, University of São Paulo, Professor Mello Moraes, 2463 São Paulo, SP, Brazil

^b Amazônia Azul Tecnologias de Defesa S.A., Corifeu de Azevedo Marques, 1847 São Paulo, SP, Brazil

^c Nuclear and Energy Research Institute, University of São Paulo, Professor Lineu Prestes, 2242 São Paulo, SP, Brazil

^d Nuclear and Industrial Engineering, Via della Chiesa XXXII 759, 55100 Lucca, Italy

ABSTRACT

Uncertainty analysis is applied in the licensing process for nuclear installations to complement best estimate analysis and to verify that the upper bound value is less than the threshold corresponding to the safety parameter of interest. Metal-water reaction is a critical safety phenomenon of water-cooled nuclear reactors at accident conditions, e.g. Loss-Of-Coolant Accidents (LOCA). AISI 348 cladding is able to increase the accident tolerance comparing to Zr-based alloys and differently from other accident tolerant fuel cladding options, there is operational experience of nuclear power plants with stainless steel. In this study, a transient oxidation experiment of AISI 348 by steam was conducted and the major sources of uncertainty were addressed. An evaluation model was developed to calculate the evolution of mass gain during the experiment. Meanwhile, uncertainty propagation of experimental data was performed. The results show that the mass gain predicted by the transient metal-water reaction model lays within the experimental data uncertainty band. Furthermore, the selection of the oxidation kinetics model seems to be important whether the analysis will provide conservative results.

1. Introduction

Significant hydrogen production results from the oxidation of Zircaloy fuel cladding by steam at elevated temperatures (Avelar et al., 2020a; Urbanic and Heidrick, 1978; Baker and Just, 1962). At severe accident conditions, the heat generated from the Zr-steam reaction can be greater than the decay heat in the core, accelerating the release of hydrogen and fission products from the damaged fuel into the containment (Avelar et al., 2023; Avelar et al., 2020b; Gauntt and Mattie, 2016).

Evaluation models present the calculation framework for evaluating the behavior of the reactor during a postulated accident or transient. They are sometimes referred to as a licensing methodology applied in the safety analysis report (USNRC, 2007a). Safety analysis rely on qualified computer codes that have embedded high temperature oxidation kinetics to simulate the consequences (in terms of heat and hydrogen generation) of the metal-water reactions. These calculations are necessary either to verify whether the acceptance criteria for Emergency Core Cooling Systems (ECCS) such as Peak Cladding Temperature (PCT) and Equivalent Cladding Reacted (ECR) are met (USNRC, 2021a), or to assess hydrogen generation during a severe

accident progression (e.g. in case of insufficient core cooling) (Avelar et al., 2023; Darnowski, Mazgaj and Włostowski, 2021; Avelar et al., 2020b).

Various options exist for combining computer codes and input data for safety analysis (IAEA, 2008). However, two main strategies are more commonly accepted by regulators. When there is a certain level of knowledge maturity and understanding regarding important phenomena, Best Estimate Plus Uncertainty (BEPU) can be introduced as safety evaluation method, in which uncertainty evaluation shall take into consideration the contributions associated to both the computer code and the input data for the code (IAEA, 2008; USNRC, 2007a). In order to provide assurance that for postulated accidents, a given plant will not exceed the applicable licensing criteria, with a probability of 95% and a 95% confidence level, statistical methods are applied to estimate uncertainty in the calculation of a BEPU analysis (IAEA, 2008; Darnowski, Mazgaj and Włostowski, 2021). On the other hand, the fully conservative approach consists to ensure that the analysis is demonstrably conservative, hence bounding the uncertainties, including those related to the limited capability of modeling important phenomena, which is based on the level of knowledge that was developed, or available, up to a specific licensing milestone. The former strategy needs a deeper

* Corresponding author.

E-mail address: alanmatiasavelar@gmail.com (A. Matias Avelar).

Table 1
Elemental composition of the austenitic stainless steel AISI 348.

| Element | Fe | Cr | Ni | Mn | Nb | Si | C | Co | N | P | Ta | S | B |
|-------------------|------|-------|-------|------|------|------|-------|-------|-------|-------|---------|-------|--------|
| Composition (wt%) | bal. | 17.45 | 10.94 | 1.61 | 0.83 | 0.42 | 0.052 | 0.023 | 0.018 | 0.017 | < 0.005 | 0.003 | 0.0007 |

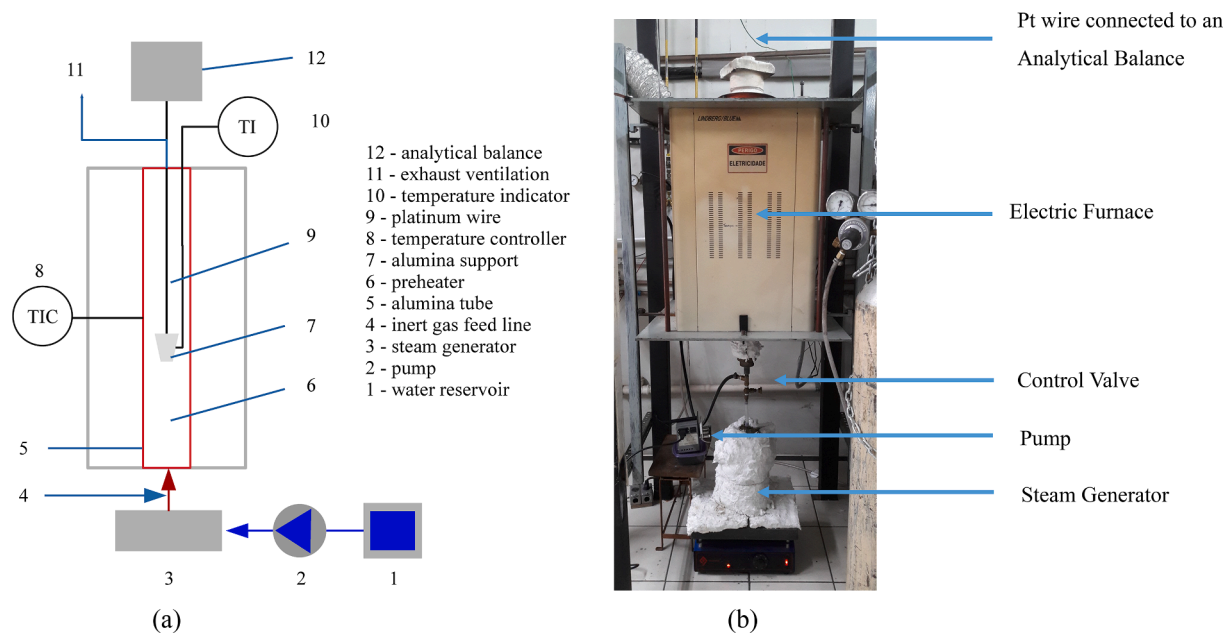


Fig. 1. (a) Schematic arrangement of steam oxidation test furnace and (b) setup of the experimental apparatus for continuous assessment of mass gain.

understanding of important phenomena, and the latter needs to prove that chosen models present safety margins to be applied for that purpose (Nelson et al., 2022; IAEA, 2008). Thus, both strategies are not applicable in the absence of relevant experimental data. Nonetheless, using probability-based uncertainty propagation informed by either simulation or experimental results needs not only the availability of experimental data, but advanced and high-fidelity modeling tools (Nelson et al., 2022).

The method to determine whether a code is capable of modelling important phenomena, e.g. metal-water reaction rate, consists of comparing the simulation results to experimental data that have known uncertainties (IAEA, 2008). Excellent agreement between the code calculation and data occurs when the calculated value is at all times within the data uncertainty band (IAEA, 2008).

The USNRC conservative approach at Design Basis at Loss-Of-Coolant Accidents (DBLOCA) analysis, ruled by the Appendix K to Part 50 ECCS Evaluation Models (USNRC, 2021b), suggests the application of Baker-Just oxidation kinetics (Baker and Just; 1962) for an estimate of hydrogen production from Zr-based fuel cladding oxidation by steam.

Among the options investigated by the coordinated research project entitled analysis of options and experimental examination of fuels for water cooled reactors with increased accident tolerance (ACTOF) (IAEA, 2020), stainless steel cladding is the only option with operational experience. Thus, it is already a reality in terms of fabrication and implementation. However, considering stainless steel fuel cladding, limited information is available about their oxidation kinetics (Avelar et al., 2020a; IAEA, 2020; Massey et al., 2016; Bittel, Sjudahl and White, 1969). In addition, there is a lack of rule selecting which metal-water reaction rate model should be applied for a conservative analysis of Fe-based alloys to verify whether applicable ECCS acceptance criteria are met. Moreover, future cladding alloys must provide an empirical database to support the applicability of reaction rate models (USNRC, 2007b).

In this context, the motivation of this work was to evaluate the magnitude of the uncertainty in the prediction of metal-water reaction rate, focusing on the development of an evaluation model applied for transient analysis of AISI 348 high temperature steam oxidation. Additionally, uncertainty propagation was performed to determine the uncertainty band. The results show that a significant variation of mass gain can be found by applying different oxidation kinetics available in the open literature (Avelar et al., 2020a; Bittel, Sjudahl and White, 1969). Bittel-White model for 304L stainless steel (Bittel, Sjudahl and White, 1969) seems appropriate for a conservative analysis of AISI 348 at LOCA scenarios.

2. Materials and methods

2.1. Experimental

The AISI 348 is an iron-based alloy, fully austenitic at room and high temperatures, which belongs to the 300 series of steels. The main difference comparing to the widely use type 304 stainless steel lies in the presence of Nb and Ta in minor concentration, to prevent sensitization by means of avoiding the formation of carbides preferentially at the grain boundaries (Tunes et al., 2019). In this study, AISI 348 disk samples with 22 mm of diameter and 2 mm of thickness were tested. The chemical composition shown in Table 1 was determined by Energy Disperse X-ray (EDX – Shimadzu™ model 800HS), Inductively Coupled Plasma Optical Emission Spectrometry (ICP-OES – PerkinElmer™ model AVIOS 500) for majors (>0.1 wt%) and minors (<0.01 wt%) elements, respectively, and the direct combustion method for carbon and sulphur (C/S Analyzer Eltra™ model CS-2000).

A high temperature oxidation apparatus with a Lindberg/Blue™ electric furnace and a steam generator to produce pure flowing steam was set up. Steam was generated by pumping distillate water from a reservoir placed underneath the furnace into a steam generator which

Table 2
Number and type of measurements.

| Number of tests | Measurements | Type |
|-----------------|--|-----------------------------|
| 6 | Furnace temperature, Internal temperature Mass gain | Continuous Discontinuous |
| 1 | Furnace temperature, Internal temperature Mass gain | Discontinuous Continuous |

was heated by a Quimis™ heating plate. Water was pumped using an Ismatec™ peristaltic pump giving approximately 1.3 mL/min. In the furnace, steam flowed into the hot zone, passing over the sample, which was positioned using an alumina crucible suspended by a platinum wire hook attached to the bottom of the Shimadzu™ analytical balance mounted above the furnace. The alumina crucible allowed catching possible scale spallation of non-adherent oxide layer. Fig. 1 (a) describes the experimental apparatus schematically and Fig. 1 (b) presents a

photograph of the experimental apparatus.

All performed tests had the same initial temperature (400 °C) and the same temperature set point to the furnace control (1300 °C). Two different configurations of measurement devices were applied, as continuous mass gain and temperature monitoring could not be performed concurrently. A total of seven runs were conducted, most of them focusing on continuous temperature measurement, according to Table 2. The experiment that measured the internal temperature evolution, did not measured continuously the sample mass gain. Sample dimensions were measured three times prior to the oxidation exposure by a Mitutoyo™ metric vernier caliper, read in millimeter and vernier scale 0.05 mm. Mass was measured three times before and three times after the experiment by a Shimadzu™ AUY220 analytical balance with 0.1 mg resolution.

Temperature data was read and recorded at each 30 s from a thermometer connected to a type K thermocouple placed inside the furnace,

Table 3
Measured parameters, calculated mass gain per area with their respective average and standard deviation (Std).

| Test | Final mass [g] | Diameter [mm] | Thickness [mm] | Mass gain per area [g/m ²] |
|---------|----------------|---------------|----------------|--|
| 1 | 4.7275 | 22.3667 | 1.5000 | 210 |
| 2 | 5.9930 | 22.2333 | 1.8167 | 229 |
| 3 | 4.7771 | 22.4333 | 1.5167 | 227 |
| 4 | 5.9871 | 22.3500 | 1.8833 | 171 |
| 5 | 6.1320 | 22.3167 | 1.9000 | 231 |
| 6 | 5.9845 | 22.3333 | 1.8000 | 241 |
| 7 | 5.9393 | 22.3500 | 1.8667 | 169 |
| Average | 5.6487 | 22.3405 | 1.7548 | 211 |
| Std | 0.6154 | 0.0600 | 0.1721 | 30 |

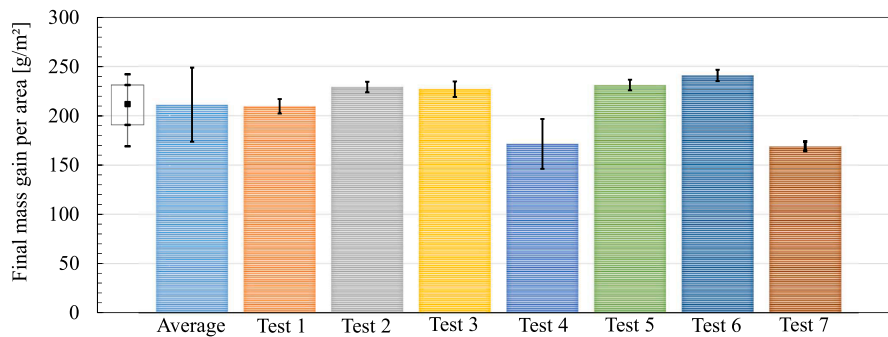


Fig. 2. Final mass gain results, the experimental combined uncertainty and box plot showing the spread of the data.

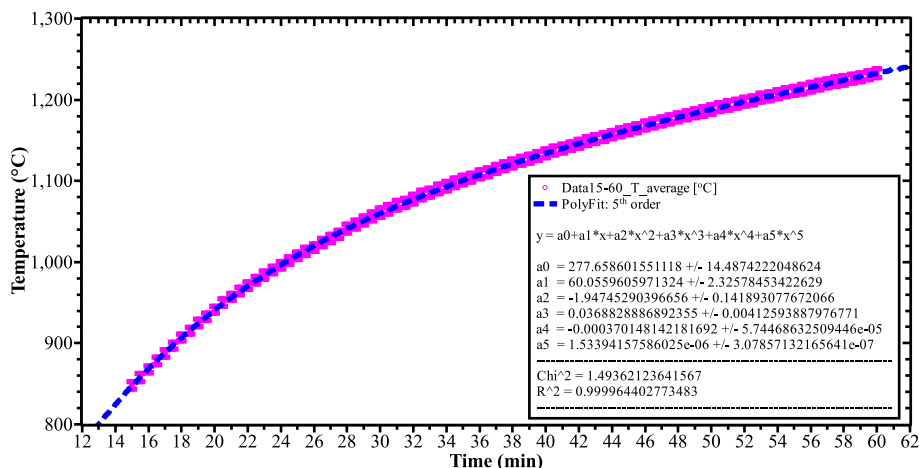


Fig. 3. Temperature time series fitted by 5th order polynomial function.

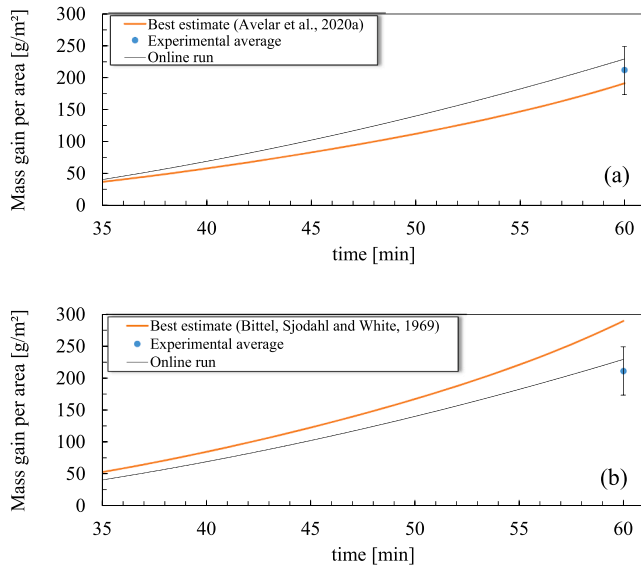


Fig. 4. Mass gain per area evolution comparing model best estimate (orange line) considering (a) AISI 348 oxidation kinetics (Avelar et al., 2020a) and (b) Bittel-White oxidation kinetics (Bittel, Sjedahl and White, 1969) against experimental results: continuous online run monitoring case (black line), mean experimental final mass gain (blue point) and uncertainty band. (For interpretation of the references to colour in this figure legend, the reader is referred to the web version of this article.)

whose measuring junction was tangent to the alumina crucible. Meanwhile, a type S thermocouple was the primary element for the furnace temperature controller. After the tests, a polynomial fit of temperature experimental data was applied to provide a continuous curve for the test.

Repeatability criteria was considered to be met at these tests as the following topics were verified (BIPM, 2008):

- Same measurement procedure.
- Same observer.
- Same measuring instrument, used under the same conditions.
- Same location.
- Repetition in a short period of time.

2.2. Uncertainty analysis of measured parameters

Uncertainty propagation was applied to evaluate uncertainties and present them alongside experimental data (Gonçalves, 2020; Taylor, 2012; BIPM, 2008). Combined mass uncertainties from initial and final mass measurements both considered the systematic mass standard uncertainty (type B) of the Shimadzu™ analytical balance of 1 mg divided by $\sqrt{3}$ due to describe by a symmetric, rectangular a priori probability distribution, and the random mass standard uncertainty (type A), which accounts one standard deviation divided by the square root of three as there were three weight measurements (BIPM, 2008).

Likewise, sample diameter and thickness combined uncertainties were both calculated considering systematic and random contributions. The systematic standard uncertainty (type B) of the Mitutoyo™ caliper rule was considered as 0.05 mm divided by $\sqrt{3}$ because it was consider the rectangular distribution. Type A standard uncertainty also accounts one standard deviation divided by the square root of three as there were three diameter or thickness measurements (BIPM, 2008).

The generic uncertainty propagation equation of a function $f = f(A, B, C, D)$ given by Eq. (1) (Gonçalves, 2020; BIPM, 2008) was applied to add in quadrature each one of the four combined uncertainties aforementioned (thickness, diameter, initial and final mass).

$$u_f = \sqrt{\left(\frac{\partial f}{\partial A}\right)^2 u_A^2 + \left(\frac{\partial f}{\partial B}\right)^2 u_B^2 + \left(\frac{\partial f}{\partial C}\right)^2 u_C^2 + \left(\frac{\partial f}{\partial D}\right)^2 u_D^2} \quad (1)$$

Where the partial derivatives are the sensitivity coefficients and the uncertainty components consider their combined uncertainty. So for $f = \Delta m/A$, Eq. (1) gives:

$$u_{\frac{\Delta m}{A}} = \sqrt{\left(\frac{\partial f}{\partial \varepsilon}\right)^2 u_\varepsilon^2 + \left(\frac{\partial f}{\partial d}\right)^2 u_d^2 + \left(\frac{\partial f}{\partial m_i}\right)^2 u_{m_i}^2 + \left(\frac{\partial f}{\partial m_f}\right)^2 u_{m_f}^2} \quad (2)$$

where ε is thickness, d is diameter, m_i is initial mass and m_f is final mass.

Lastly, the expanded uncertainty was obtained as the combined mass gain per area uncertainty was multiplied by a coverage factor (k_{95}) to expand uncertainty to a 95% confidence interval, considering Student's T table with an effective degrees of freedom (ν_{eff}) obtained from the Welch-Satterwaite equation (BIPM, 2008).

Similar calculation was performed considering temperature measurements. The type K thermocouples were considered to provide a type B standard uncertainty of 0.75% of the measured temperature. Thermometer precision was considered to add a systematic component (type B) of 0.1% of the measured temperature plus 2 °C divided by $\sqrt{3}$ due to rectangular distribution. Temperature standard deviation was calculated at each time step considering the temperature time series. Type A standard uncertainty considered the mean standard deviation divided by the square root of the number (N) of temperature series that were taken into account. The expanded temperature uncertainty was obtained as the combined temperature uncertainty was multiplied by a coverage factor (k_{95}) to expand uncertainty to a 95% confidence interval, considering Student's T table with a degrees of freedom $\nu = N - 1$ (BIPM, 2008).

2.3. Transient metal-water reaction model

A metal-water oxidation model developed using Scilab and Excel Visual Basic for Applications (VBA) was applied to perform transient analysis of the experiment. The model has two inputs: temperature evolution and metal-water oxidation kinetics. The output is mass gain evolution throughout steam exposure time. Transient oxidation is calculated by Eq. (3), where n is equal 1 for linear and 2 for parabolic kinetics, for example.

$$\frac{d(\frac{\Delta m}{A})}{dt} = \frac{1}{n} \left(A e^{-\frac{E}{RT}} \right)^{\frac{1}{n}} t^{\left(\frac{1}{n}-1\right)} \quad (3)$$

where $\Delta m/A$ is mass gain per unit area, t is time, A is pre-exponential factor, E is activation energy of the oxidation reaction, R is the gas constant, and T is temperature. For non-linear rate models, the rate of layer growth may be controlled by other phenomena, e.g. ionic diffusion, and time shall be corrected to the equivalent isothermal oxidation time (t') according to Eq. (4) to allow evaluating reaction rate accurately.

$$t' = \frac{\left(\frac{\Delta m}{A}\right)_{t=dt}}{\left(A e^{-\frac{E}{RT}}\right)^n} \quad (4)$$

Considering AISI 348, mass gain rate in $g\ mm^{-2}\ s^{-1}$ may be calculated by Eq. (5) (Avelar et al., 2020a).

$$\frac{d(\frac{\Delta m}{A})}{dt} = \frac{1}{2} \left(4.85 \times 10^1 e^{\left(\frac{-41338+1257}{T \pm u_T [K]}\right)} \right)^{\frac{1}{2}} t' [s]^{\left(-\frac{1}{2}\right)} \quad (5)$$

Considering Bittel-White (1969) kinetics for 304L stainless steel, mass gain rate in $g\ mm^{-2}\ s^{-1}$ may be calculated by Eq. (6) (Bittel, Sjedahl and White, 1969).

Table 4
Uncertainty parameters and distributions selected for the study.

| Case | Oxidation kinetics | Parameter | Distribution | Distribution Parameters | Distribution Values | Unit |
|------|---------------------------------------|-----------|--------------|-------------------------|-------------------------------------|------|
| 1 | Avelar et al. (2020a) | E/R | Normal | | 41,338 628.5 | K |
| 2 | Avelar et al. (2020a) | T | Normal | Mean | Poly. Func. 14.6 | K |
| 3 | Bittel-White (1969) | E/R | Normal | Std | 42,450 604 | K |
| 4 | Bittel-White (1969) | T | Normal | | Poly. Func. 14.6 | K |
| 5 | Avelar et al. (2020a) | E/R | Uniform | | 40,081 42,595 | K |
| 6 | Avelar et al. (2020a) | T | Uniform | | Poly. Func. -29 Poly. Func. + 29 | K |
| 7 | Bittel-White (1969) | E/R | Uniform | Upper and lower limits | 41,242 43,658 | K |
| 8 | Bittel-White (1969) | T | Uniform | | Poly. Func. -29 Poly. Func. + 29 | K |

$$\frac{d\left(\frac{\Delta m}{A}\right)}{dt} = \frac{1}{2} \left(2.4 \times 10^2 e^{\left(\frac{-42450 \pm 1208}{T \pm 17 [K]}\right)} \right)^{\frac{1}{2}} t^{\left(\frac{1}{2}\right)} \quad (6)$$

Numerical integration was applied to accumulate mass gain through the simulation time. At each time step, mass gain was calculated according to Eq. (7) by considering the trapezoidal rule.

$$\left(\frac{\Delta m}{A}\right)\Big|_t = \left(\frac{\Delta m}{A}\right)\Big|_{t-dt} + \left(\frac{\frac{d\left(\frac{\Delta m}{A}\right)}{dt}\Big|_t + \frac{d\left(\frac{\Delta m}{A}\right)}{dt}\Big|_{t-dt}}{2} \right) dt \quad (7)$$

Model calculation were performed considering both oxidation kinetics ([Avelar et al., 2020a](#); [Bittel, Sjudahl and White, 1969](#)). Afterwards, calculation was repeated considering the activation energy uncertainty from the oxidation kinetics and temperature uncertainty from the experiment, to provide the model uncertainty range.

3. Results and discussion

First, experimental results were analyzed and their uncertainty were propagated to determine the uncertainty band of mass gain per area. Meanwhile, the transient oxidation model was applied to provide an estimate of the mass gain per area evolution throughout the entire steam exposure time. Different input data was applied, including different oxidation kinetics, temperature evolution and activation energy.

Second, both results were compared to verify the model applicability. In other words, the agreement between the model calculation, the experimental data and its uncertainty band was assessed.

3.1. Mass gain uncertainty

Propagation of uncertainty was performed taking into account the four measured parameters to allow the calculation of mass per area uncertainty of each experiment. Then, the type A standard uncertainty was assessed considering one standard deviation divided by the square root of seven as there were seven tests.

[Table 3](#) shows the mean results of diameter, thickness and final mass from the measurements of each test, the calculated mass gain per area and the average and standard deviation considering the seven performed tests. [Fig. 2](#) presents a comparison of the final mass gain per area results obtained at each test against the average value and their respective combined uncertainty. It shows that individual test uncertainty are less than the random uncertainty, indicating that the temperature evolution of each test sample could have been different. The box plot represents the middle 50% of the experimental results.

3.2. Temperature uncertainty

Two temperature series were not considered as the thermocouple position at the two first test was not considered appropriate, as the measurement was not tangent to the alumina crucible. It is important that the measurement can express the sample temperature evolution as accurate as possible as the reaction that took place is exothermic ([Avelar et al., 2020a](#)) and a temperature boundary layer is expected to exist between the sample surface and the steam flow. Temperature overshoot discussion considering Zircaloy-4 metal-water reaction was assessed by Carthcart-Pawel ([Carthcart et al., 1977](#)).

Nonetheless, four temperature-time series were considered to provide enough number of points for the polynomial function of order 5. [Fig. 3](#) presents the polynomial function, which provided the best fit to the experimental data using Levenberg-Marquardt method weighted by uncertainty. The temperature evolution adjust was revisited considering F statistic results. The polynomial function of 5th order showed no significant statistical difference comparing to 6th order for a 99% confidence interval. The polynomial function was applied in the non-isothermal oxidation model to predict the mass gain evolution.

3.3. Model best estimate and uncertainty

The mass gain per area expanded uncertainty was plotted against the model centerline in order to verify the applicability of the code ([IAEA, 2008](#)). [Fig. 4 \(a\)](#) presents the results considering AISI 348 oxidation kinetics ([Avelar et al., 2020a](#)) whereas [Fig. 4 \(b\)](#) presents the results with Bittel-White model ([Bittel, Sjudahl and White, 1969](#)). In both figures, the best estimate curve (orange line) given by each kinetic model is

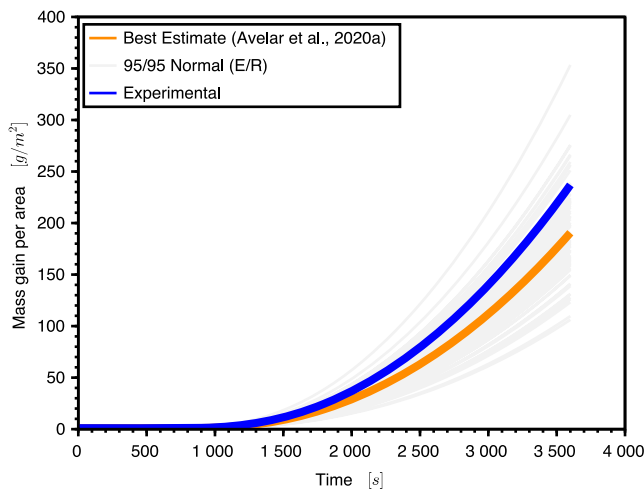


Fig. 5. Evolution of the AISI 348 mass gain during the temperature transient comparing experimental results and simulations of case 1, considering normal distribution of the activation energy uncertainty and AISI 348 oxidation kinetics (Avelar et al., 2020a).

compared against the experimental results for continuous monitoring of mass gain (online run - black line), mean experimental final mass gain (blue point) and uncertainty band.

The results indicate that both oxidation kinetics are applicable but with different degrees of agreement between model and data. For AISI 348 oxidation kinetics (Avelar et al., 2020), excellent agreement between model and data (IAEA, 2008) was found. While considering Bittel-White model (Bittel, Sjødahl and White, 1969), the calculation shows the same trends as the data, indicating a reasonable agreement (IAEA, 2008).

To introduce the uncertainties in the calculation through the input data for the code (IAEA, 2008; USNRC, 2007a), two parameters were considered: activation energy and temperature. Uniform and normal distributions were applied for both parameters and for both oxidation kinetics. The probability distribution functions and its parameters are presented in Table 4. The best estimate parameters are considered as the mean value for both normal and uniform distributions. The Best

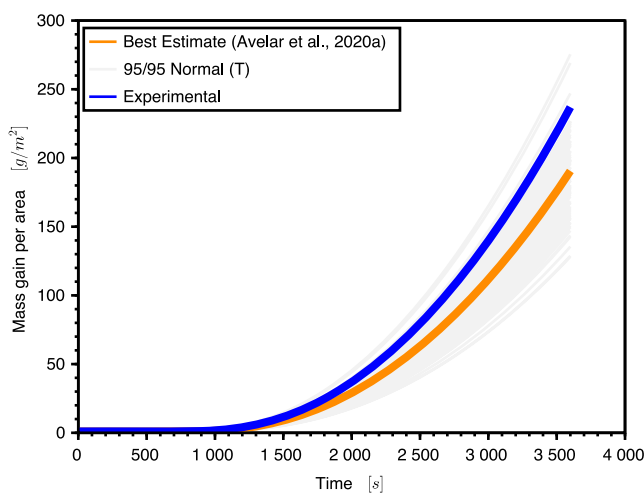


Fig. 6. Evolution of the AISI 348 mass gain during the temperature transient comparing experimental results and simulations of case 2, considering normal distribution of the temperature uncertainty and AISI 348 oxidation kinetics (Avelar et al., 2020a).

Estimate Plus Uncertainty Oxidation Model Scilab code for normal distribution of the studied parameters is available in the Appendix A. An input deck with 93 cases was generated for each uncertainty test in order to provide the two-sided 95%/95% probability and confidence level for two-sided coverage of the distribution (Darnowski, Mazgaj and Wiosowski, 2021). The temperature distribution values were calculated considering the mean and combined uncertainty derived from the polynomial coefficients' uncertainties shown in Fig. 3, for normal distribution. On the other hand, for uniform distribution, the limits were defined by the expanded uncertainty with a 95% confidence interval, i.e. one standard deviation (Std) multiplied by the Student's T table coverage factor, considering the total number of experimental data points minus the polynomial order plus one as degrees of freedom.

Fig. 5 and Fig. 6 show the results for Avelar et al. (2020a) considering activation energy and temperature uncertainties, respectively. The experimental curve presents the online run test, where the mass sample was continuously measured. Fig. 7 presents a comparison of the distributions of the final experimental mass gain against the distribution of simulation cases 1 and 2. Although the model shows a tendency to under-predict the mass gain, the simulation results for both uncertainty parameters are wide enough to comprehend the experimental results.

The same analysis was applied to Bittel-White model (Bittel, Sjødahl and White, 1969) in cases 3 and 4. Fig. 8 and Fig. 9 show the results considering activation energy and temperature uncertainties, respectively. Fig. 10 presents a comparison of the distributions of the final experimental mass gain against the distribution of simulation cases 3 and 4.

Although the Avelar et al. (2020a) model calculated values lie within the data uncertainty band, this model presents a tendency to under-predict the mass gain. However, the simulation results for both uncertainty parameters were wide enough to comprehend the distribution of the experimental results.

On the other hand, the Bittel-White model (Bittel, Sjødahl and White, 1969) shows a tendency to over-predict the mass gain. Differently to the other model, the simulation results for temperature uncertainty were not wide enough to comprehend the experimental results. Nevertheless, the activation energy uncertainty from both models was capable of comprising the experimental results. The results for cases 5 to 8 with uniform distribution are included in the Appendix B.

Each one of the selected uncertainty parameters are already significant individually. Together they would produce a synergistic effect, increasing the final uncertainty. The temperature uncertainty becomes more important the higher is the activation energy. Thus, although the experiment tried to replicate the same temperature evolution, a small error in the temperature provides a faster reaction, which generates more heat by metal-water reactions that took place, which are exothermic and creates a chain effect. Coupling these uncertainties results in a much wider model spread than the experimental uncertainty band.

A more precise result, i.e. small random error, would have been noticed whether more tests were performed. However, despite the significant mass gain per area uncertainty, the model uncertainty overcomes the experimental uncertainty. Thus, the experimental uncertainty with the current apparatus was considered to be within the desired limit of error.

Considering the experimental data set, a new transient oxidation model for stainless steel was developed to provide better adjust to the non-isothermal oxidation of AISI 348, according to Eq. (8), where mass gain rate in $g\ mm^{-2}\ s^{-1}$. The results for the new model are shown in Fig. 11 and Fig. 12 considering activation energy and temperature uncertainties, respectively. The comparison of the final mass gain results considering normal distribution of uncertainty parameters against the distribution of the experimental data is presented in Fig. 13. The new oxidation model was developed considering the continuous thermo gravimetric analysis. Its predictions cover the upper bound of the

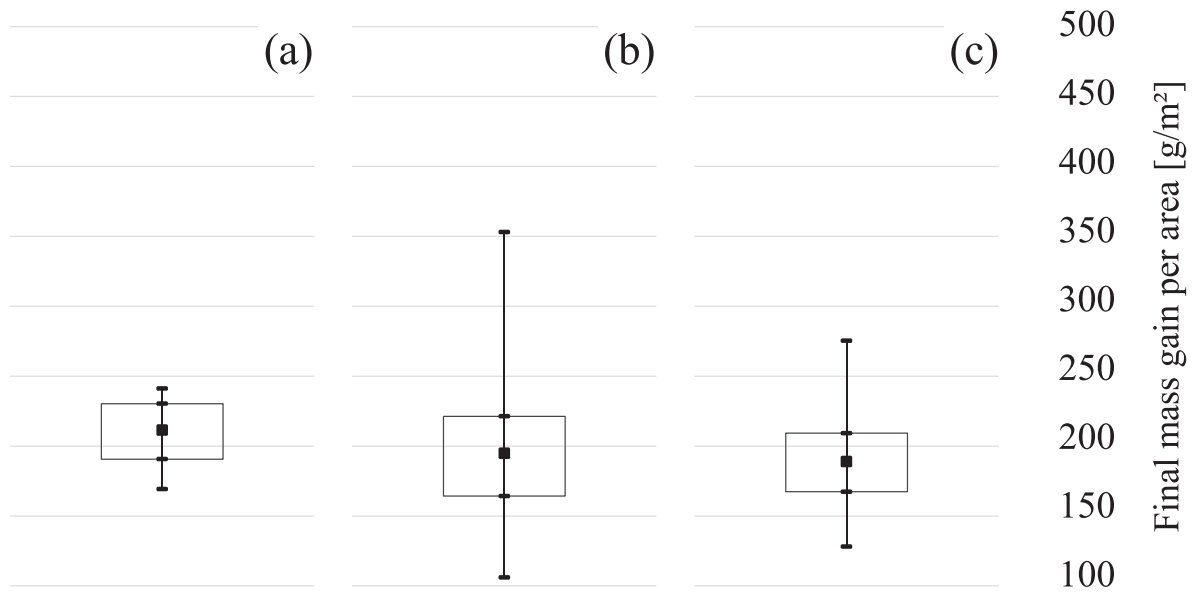


Fig. 7. Box plot with the distribution of the final experimental mass gain (a) comparing with the distributions of simulation case 1 (b) and case 2 (c).

experimental results in order to correct possible difference noticed between hydrogen generation and sample mass gain in ACTOF project (IAEA, 2020).

$$\frac{d\left(\frac{\Delta m}{A}\right)}{dt} = \frac{1}{2} \left(4.85 \times 10^1 e^{\left(\frac{-40700+1000}{T \pm u_T [K]}\right)} \right)^{\frac{1}{2}} t^{\left(-\frac{1}{2}\right)} \quad (8)$$

Whether the analysis indeed will provide conservative results, the oxidation kinetics selection plays a major role. For example, Darnowski et al. (2021) showed that applying Baker-Just oxidation kinetics for Zr-based cladding resulted in a higher hydrogen production for PWR models. Thus, it is possible make an analogy for AISI 348 cladding, for example, in the context of ECCS acceptance criteria analysis. Bittel-White model for stainless steel oxidation by steam (Bittel, Sjodahl and White, 1969) may be applied instead of Baker-Just model for Zr-based cladding (USNRC, 2021b) for a conservative estimate of cladding

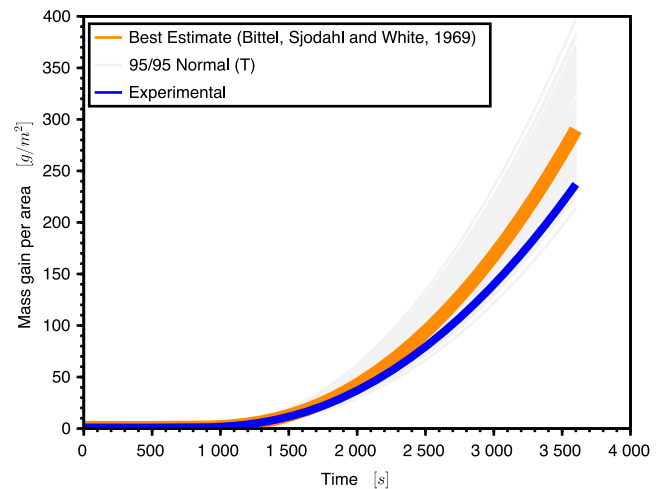


Fig. 9. Evolution of the AISI 348 mass gain during the temperature transient comparing experimental results and simulations of case 4, considering normal distribution of the temperature uncertainty and Bittel-White model (Bittel, Sjodahl and White, 1969).

oxidation and hydrogen generation.

3.4. Inter-laboratory comparison

Recently, the International Atomic Energy Agency (IAEA) published a report with experimental results of high temperature oxidation of Cr-coated Zr-based alloys and Fe-based alloys. At least 3 different laboratories run a similar reaction rate experiments in a coordinated research project related to the analysis of options and experimental examination of fuels for water cooled reactors with increased accident tolerance (ACTOF) (IAEA, 2020).

Reproducibility usually refers to the degree of agreement between the results of experiments conducted by different individuals, at different locations, with different instruments (BIPM, 2008). In this context, ACTOF (IAEA, 2020) results provide inter-laboratory

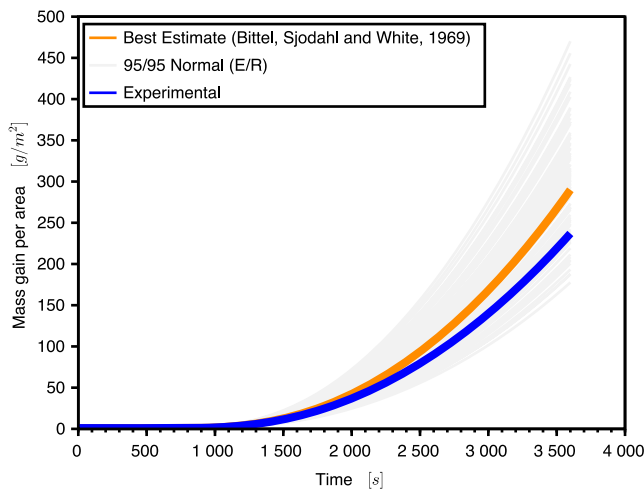


Fig. 8. Evolution of the AISI 348 mass gain during the temperature transient comparing experimental results and simulations of case 3, considering normal distribution of the activation energy uncertainty and Bittel-White model (Bittel, Sjodahl and White, 1969).

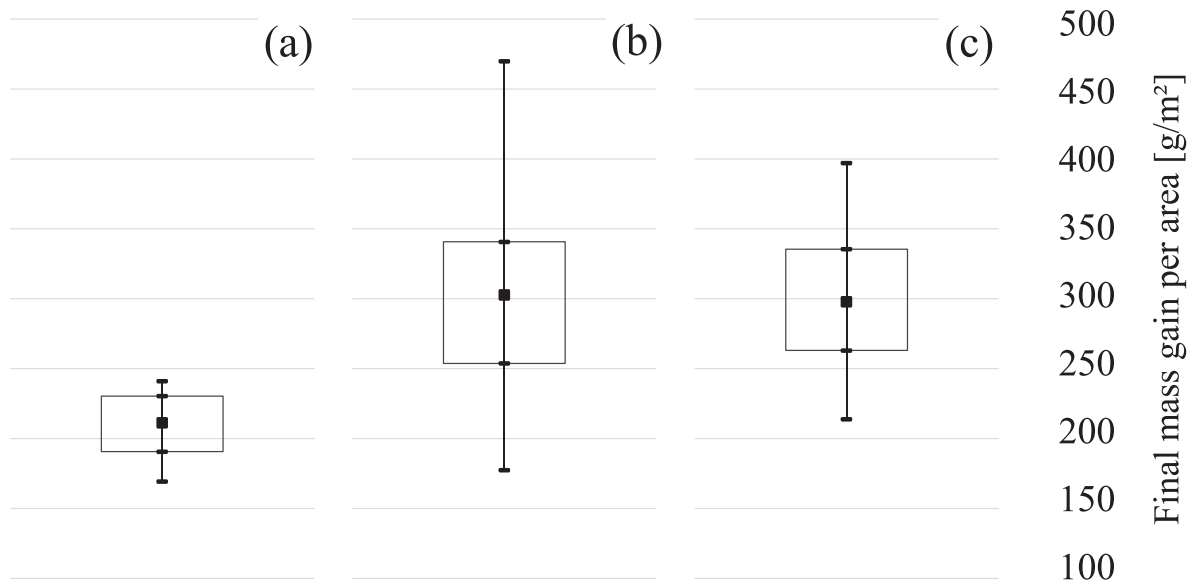


Fig. 10. Box plot with the distribution of the final experimental mass gain (a) comparing with the distributions of simulation case 3 (b) and case 4 (c).

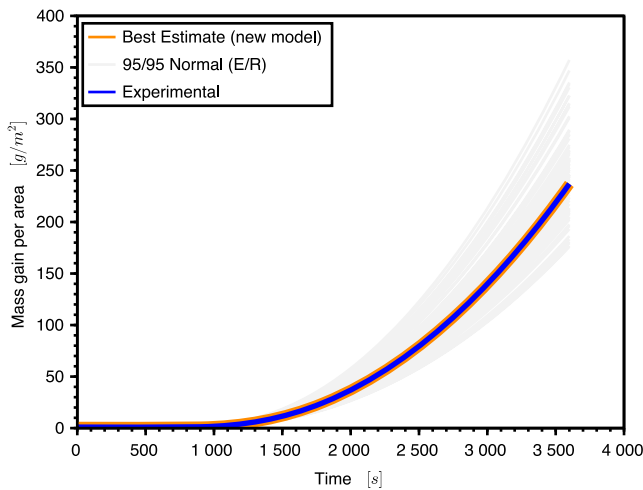


Fig. 11. Evolution of the AISI 348 mass gain during the temperature transient comparing experimental results and simulations cases for the new non-isothermal oxidation model, considering normal distribution of the activation energy uncertainty.

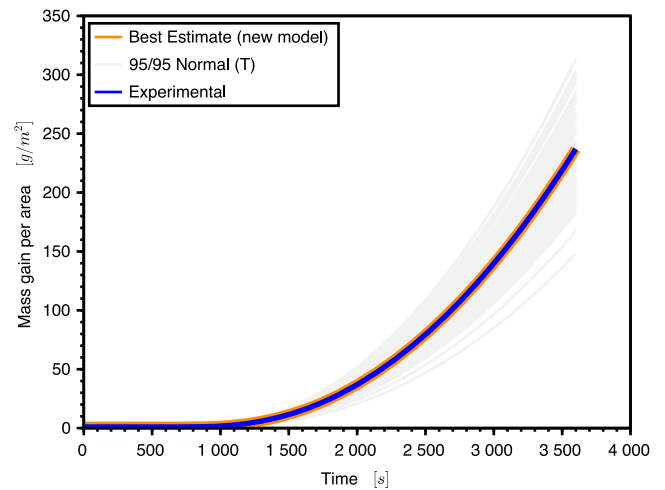


Fig. 12. Evolution of the AISI 348 mass gain during the temperature transient comparing experimental results and simulations cases for the new non-isothermal oxidation model, considering normal distribution of the temperature uncertainty.

comparison of AISI 348 high temperature steam oxidation.

Some testing parameters vary among laboratories, such as the heating rates, steam flow rates, quench parameters, temperature measurements, and sample holders, for example. In addition, different laboratories and setups can measure different parameters such as hydrogen production or online mass changes.

It is possible to convert the mass gain results into hydrogen generation using a simple relationship applicable for steam oxidation (Avelar et al, 2020a). Table 5 presents hydrogen generation results from AISI 348 reaction with steam, either from an estimative from experimental mass gain data or kinetic model or direct hydrogen measurement.

To the best of the authors' knowledge, none of the experimental results (Avelar et al., 2020a; IAEA, 2020) surpass the predictions given by Bittel-White model for stainless steel oxidation by steam (Bittel, Sjodahl and White, 1969). Thus, considering a transient analysis, the

higher reaction rates given by Bittel-White tend to leave the data uncertainty band for AISI 348, as shown in Fig. 4. The predictions given by new oxidation model are given for comparison in Table 5.

4. Conclusions

Among the fuel cladding options being assessed for water cooled reactors with increased accident tolerance (IAEA, 2020), AISI 348 is a candidate with operational experience, as stainless steel used to be the fuel cladding in the first nuclear reactors (Terrani et al., 2014). However, there is a lack of regulation regarding Fe-based cladding and usual embrittlement criteria during LOCA is not applicable for future cladding alloys (Goodson and Geelhood, 2020). This study investigated the non-isothermal steam oxidation of AISI 348 and developed a numerical model capable of predicting its mass gain evolution. The following conclusions were drawn:

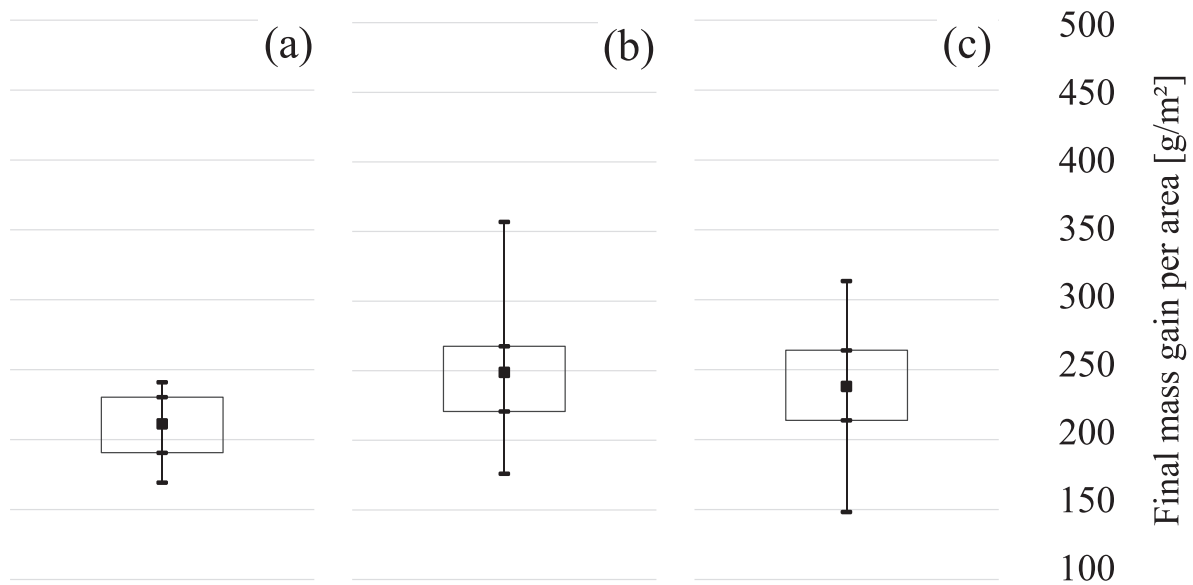


Fig. 13. Box plot with the distribution of the final experimental mass gain (a) comparing with the distributions of simulations cases for the new non-isothermal oxidation model, considering the activation energy uncertainty (b) and temperature uncertainty (c).

Table 5

Inter-laboratory comparison of hydrogen generation from AISI 348 reaction with steam at high temperatures (IAEA, 2020; Avelar et al., 2020a; Bittel, Sjudahl and White, 1969).

| t [s] | T [°C] | H ₂ generated [g/m ²] | | | | | | | |
|-------|--------|--|------------------|------------------|------------------|------------------|------------------------------------|----------------------------------|-------------------------|
| | | IAEA (2020) | | | | | Avelar et al. (2020a) ² | Bittel-White (1969) ² | This study ² |
| | | KIT ¹ | KIT ¹ | KIT ² | CTU ² | VTT ² | | | |
| 3600 | 1100 | 21.1 | 20 | 17.6 | 14.1 | 9.2 | 9.7 – 24.2 | 14.6 – 35.2 | 13.4 – 27.8 |
| 1800 | 1200 | 44.3 | 42 | 40.3 | 11.8 | 26.8 | 19.6 – 46.0 | 30.4 – 69.0 | 26.6 – 52.4 |
| 300 | 1300 | 30.2 | 27 | 28.1 | 21.3 | 33 | 20.1 – 44.6 | 31.8 – 68.6 | 26.7 – 50.3 |

¹ measured directly the hydrogen generation (IAEA, 2020).

² prediction range calculated from mass gain data (Avelar et al, 2020b).

1. The model presents good agreement with the experimental results and is capable of predicting the mass gain within the data uncertainty band. On the other hand, Bittel-white oxidation kinetics for 304 stainless steel (Bittel, Sjudahl and White, 1969) is demonstrably conservative for AISI 348 and its predictions tend to escape from the data uncertainty band.
2. Both activation energy uncertainties (Avelar et al., 2020a; Bittel, Sjudahl and White, 1969) comprise the experimental uncertainties. Noticeably, the higher is the activation energy, the more significant is the effect of temperature uncertainty.
3. A new non-isothermal oxidation model was developed for AISI 348 metal-water reaction. Its predictions provide a better estimate of the transient oxidation experiment comparing to other models (Avelar et al., 2020a; Bittel, Sjudahl and White, 1969). Meanwhile, it gives good agreement with round-robin isothermal tests.
4. For a conservative analysis of ECCS acceptance criteria considering AISI 348 cladding, Bittel-White model for stainless steel oxidation by steam (Bittel, Sjudahl and White, 1969) may be applied as an analogy of Baker-Just model for Zr-based cladding (USNRC, 2021b). Bittel-White model (Bittel, Sjudahl and White, 1969) seems appropriate for a conservative analysis of AISI 348 at LOCA scenarios regarding not only the results from this study but also the experimental results from the ACTOF report (IAEA, 2020).

CRediT authorship contribution statement

Alan Matias Avelar: Conceptualization, Investigation, Resources, Software, Writing – original draft. **Camila Diniz:** Conceptualization, Investigation, Software. **Fábio de Camargo:** Methodology, Writing – review & editing. **Claudia Giovedi:** Methodology, Writing – review & editing. **Alfredo Abe:** Writing – review & editing. **Marco Cherubini:** Methodology, Writing – review & editing. **Alessandro Petruzzi:** Methodology, Supervision. **Marcelo Breda Mourão:** Methodology, Project administration, Writing – review & editing, Supervision.

Declaration of Competing Interest

The authors declare that they have no known competing financial interests or personal relationships that could have appeared to influence the work reported in this paper.

Data availability

Data will be made available on request.

Acknowledgements

The authors acknowledge the support from CAPES and CNPq.

Appendix A. Best estimate plus uncertainty oxidation model Scilab code

```

//Best Estimate Plus Uncertainty Analysis of Transient Metal-Water Reaction

clear
clc
A=4.85e7
dma(1)=0.001
dt=1
t(1)=1e-3
scf()

//generating 93 input
mean_ER = 40700
std_ER = 500
vector_ER = mean_ER+ std_ER*rand(1,93,['normal'])
for j=1:1:93
    ER=vector_ER(j)
//Non-isothermal
for i=1:1:3600
    T=(277.658601551118+60.0559605971324*(t(i)/60)-
1.94745290396656*(t(i)/60)^2+0.0368828886892355*(t(i)/60)^3-
0.000370148142181692*(t(i)/60)^4+1.53394157586025e-06*(t(i)/60)^5)+273.15
    teq=dma(i)^2/(A*exp(-ER/T))
    dmar(i)=(1/2*sqrt(A*exp(-ER/T))*1/teq^(1/2)+1/2*sqrt(A*exp(-ER/T))*1/(teq-0.1)^(1/2))/2
    dma(i+1)=dma(i)+dmar(i)*dt
    t(i+1)=t(i)+dt
end
// g/m²
//h2=126.*dma
fdma(j)=dma(3600)*1000
gca().thickness =1
plot2d (t,dma*1000,style=[color("gray95");1])
end

ER=40700
//Non-isothermal
for i=1:1:3600
    T=(277.658601551118+60.0559605971324*(t(i)/60)-
1.94745290396656*(t(i)/60)^2+0.0368828886892355*(t(i)/60)^3-
0.000370148142181692*(t(i)/60)^4+1.53394157586025e-06*(t(i)/60)^5)+273.15
    teq=dma(i)^2/(A*exp(-ER/T))
    dmar(i)=(1/2*sqrt(A*exp(-ER/T))*1/teq^(1/2)+1/2*sqrt(A*exp(-ER/T))*1/(teq-0.1)^(1/2))/2
    dma(i+1)=dma(i)+dmar(i)*dt
    t(i+1)=t(i)+dt
end
// g/m²
//h2=126.*dma
plot2d (t,1000*dma,style=[color("darkorange");1])
BE=gca().children.children(1)

```

```

BE.thickness=4

//Experimental
A=4.85e7
ER=40700
for i=1:1:3600
    T=(277.6586015511118+60.0559605971324*(t(i)/60)-
    1.94745290396656*(t(i)/60)^2+0.0368828886892355*(t(i)/60)^3-
    0.000370148142181692*(t(i)/60)^4+1.53394157586025e-06*(t(i)/60)^5)+273.15
    teq=dma(i)^2/(A*exp(-ER/T))
    dmar(i)=(1/2*sqrt(A*exp(-ER/T))*1/teq^(1/2)+1/2*sqrt(A*exp(-ER/T))*1/(teq-1)^(1/2))/2
    dma(i+1)=dma(i)+dmar(i)*dt
    t(i+1)=t(i)+dt
end
plot2d (t,1000*dma,style=[2;1])
EXP=gca().children.children(1)
EXP.thickness=2

gca().box="on"
gca().font_size=3
xlabel(['Time ' '$[s]$', 'fontsize',3])
ylabel(['Mass gain per area ' '$[g/m^2]$', 'fontsize',3])
legends(["Best Estimate (new model)";"95/95 Normal
(E/R)";"Experimental"],[color("darkorange");1],[color("gray95");1],[2;1]],with_box=1,opt=2,font_size=3)

```

Appendix B. Results for uniform distribution cases

As discussed above, uniform distribution was applied to cases 5 up to 8. The idea of having an uniform uncertainty distribution is a more conservative approach comparing to other probability distribution functions. As hydrogen generation calculations arises from metal-water oxidation kinetics, it may be interesting to assess the extension of possible results through a conservative approach, especially in the absence of a relevant quantity of experimental data.

Fig. 14 and Fig. 15 show the results for Avelar et al. (2020a) considering activation energy and temperature uncertainties, respectively. Fig. 16 and Fig. 17 show the results for Bittel-White model (Bittel, Sjudahl and White, 1969) considering activation energy and temperature uncertainties, respectively.

The advantages of a uniform distribution are as follows:

- Extremely simple.
- Reduced computational time.
- Directly provides the worst scenario.

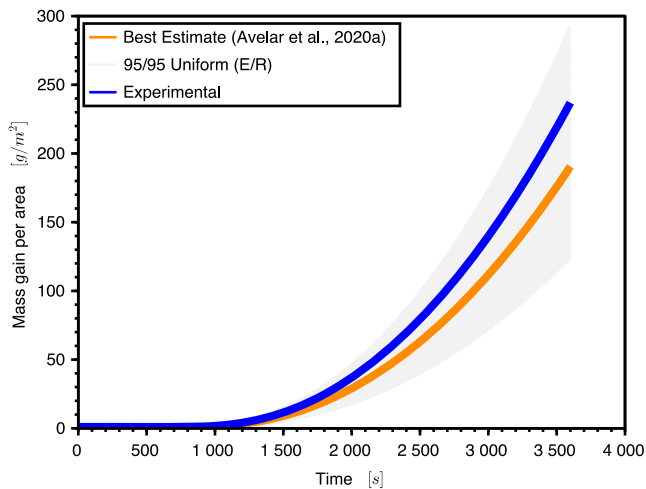


Fig. 14. Evolution of the AISI 348 mass gain during the temperature transient comparing experimental results and simulations of case 5, considering uniform distribution of the activation energy uncertainty and AISI 348 oxidation kinetics (Avelar et al., 2020a).

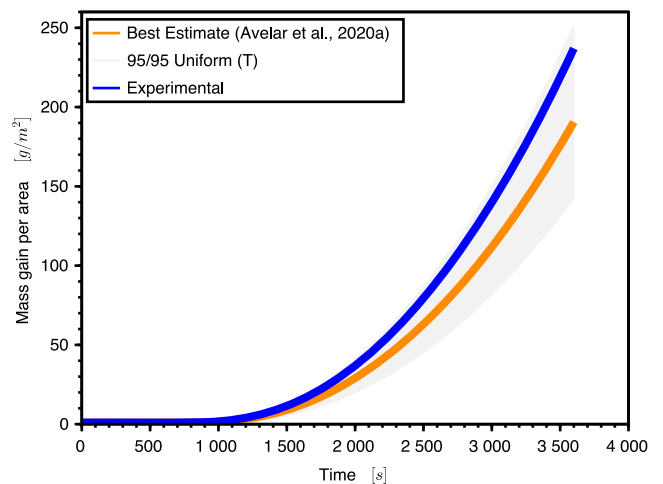


Fig. 15. Evolution of the AISI 348 mass gain during the temperature transient comparing experimental results and simulations of case 6, considering uniform distribution of the temperature uncertainty and AISI 348 oxidation kinetics (Avelar et al., 2020a).

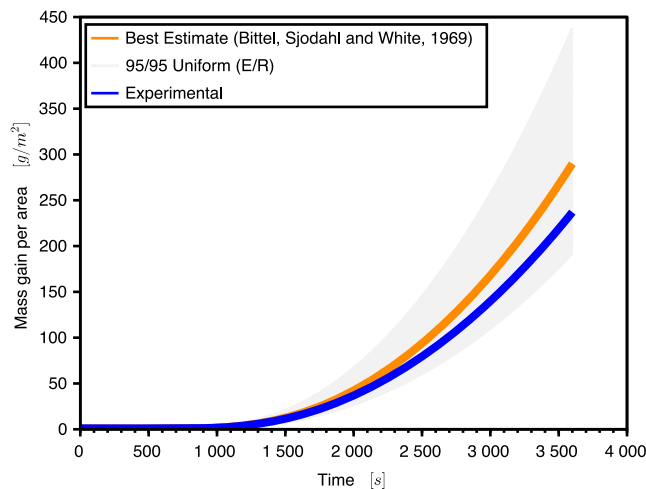


Fig. 16. Evolution of the AISI 348 mass gain during the temperature transient comparing experimental results and simulations of case 7, considering uniform distribution of the activation energy uncertainty and Bittel-White model (Bittel, Sjudahl and White, 1969).

References

- Avelar, A.M., de Camargo, F., da Silva, V.S.P., Giovedi, C., Abe, A.Y., Mourão, M.B., 2023. Effectiveness of Ni-based and Fe-based cladding alloys in delaying hydrogen generation for small modular reactors with increased accident tolerance. *Nucl. Eng. Technol.* 15 (1), 156–168. <https://doi.org/10.1016/j.net.2022.09.002>.
- Avelar, A.M., Giovedi, C., Abe, A.Y., Mourão, M.B., 2020a. Oxidation of AISI 304L and 348 Stainless Steels in Water at High Temperatures. *Mater. Res.* 23 (6), e20200373. <https://doi.org/10.1590/1980-5373-MR-2020-0373>.
- Avelar, A.M., Mourão, M.B., Maturana, M., Giovedi, C., Abe, A.Y., Pedrassani, R., Su, J., 2020b. On the nuclear safety improvement by post-inerting small modular reactor with stainless steel cladding. *Ann. Nucl. Energy* 149, 107775. <https://doi.org/10.1016/j.anucene.2020.107775>.
- Baker, L.J., Just, L.C., 1962. Studies of metal-water reactions at high temperatures experimental-and theoretical studies of the zirconium-water reaction AEC Research and Development Report (Report No.: ANL-6548). <https://doi.org/10.2172/4781681>.
- BIPM, 2008. Evaluation of measurement data — Guide to the expression of uncertainty in measurement. https://www.bipm.org/documents/20126/2071204/JCGM_100_2008_E.pdf/cb0ef43f-baa5-11cf-3f85-4dcd86f77bd6 (accessed 17 august 2022).
- Cathcart, J.V., Pawel, R.E., McKee, R.A., Druschel, R.E., Yurek, G.J., Campbell, J.J., et al., Zirconium Metal-Water Oxidation Kinetics, IV: Reaction Rate Studies (Report No.: ORNL/NUREG-17). <https://doi.org/10.2172/7317596>.
- Bittel, J.T., Sjudahl, L.H., White, J.F., 1969. Oxidation of 304L stainless steel by steam and by air. *Corrosion* 25 (1), 7–14. <https://doi.org/10.5006/0010-9312-25.1.7>.
- Darnowski, P., Mazgaj, P., Wlostowski, M., 2021. Uncertainty and Sensitivity Analysis of the In-Vessel Hydrogen Generation for Gen-III PWR and Phebus FPT-1 with MELCOR 2.2. *Energies* 14 (16), 4884. <https://doi.org/10.3390/en14164884>.
- Gauntt, R.O., Mattie, P.D., 2016. Fukushima Daiichi Unit 1 Accident Progression Uncertainty Analysis and Implications for Decommissioning of Fukushima Reactors - Volume I (Report No.: SAND2016-0232). <https://doi.org/10.2172/1235213>.
- Gonçalves, L.M., 2020. Only those who experiment make errors, and who experiments, errs! a manifesto for the calculation of the propagation of uncertainties. *Quim. Nova* 43 (2), 249–252. <https://doi.org/10.21577/0100-4042.20170460>.
- Goodson, C.E., Geelhood, K.J., 2020. Degradation and Failure Phenomena of Accident Tolerant Fuel Concepts (Report No.: PNNL-30445). <https://www.nrc.gov/docs/ML1903/ML19036A716.pdf> (accessed 21 september 2022).
- IAEA, 2008. Best Estimate Safety Analysis for Nuclear Power Plants: Uncertainty Evaluation. (Safety Reports Series No. 52). <https://www.iaea.org/publications/776>

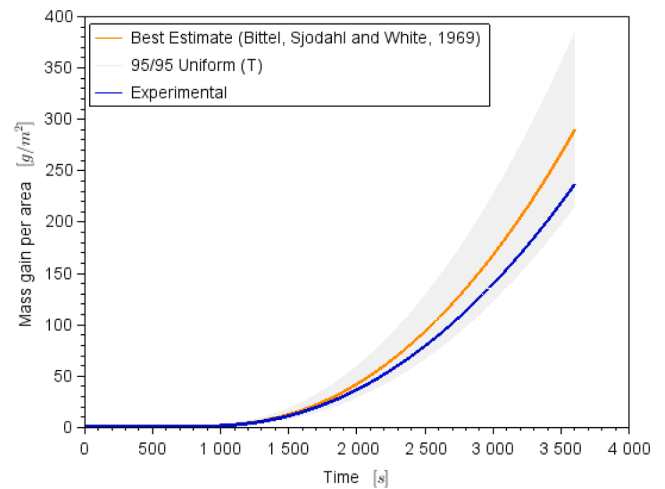


Fig. 17. Evolution of the AISI 348 mass gain during the temperature transient comparing experimental results and simulations of case 8, considering uniform distribution of the temperature uncertainty and Bittel-White model (Bittel, Sjudahl and White, 1969).

- [8/best-estimate-safety-analysis-for-nuclear-power-plants-uncertainty-evaluation](https://www.iaea.org/publications/14691/analysis-of-options-and-experimental-examination-of-fuel-s-for-water-cooled-reactors-with-increased-accident-tolerance-actof) (accessed 21 september 2022).
- IAEA, 2020. Analysis of Options and Experimental Examination of Fuels for Water Cooled Reactors with Increased Accident Tolerance (ACTOF): Final Report of a Coordinated Research Project (Report No.: IAEA-TECDOC-1921). <https://www.iaea.org/publications/14691/analysis-of-options-and-experimental-examination-of-fuel-s-for-water-cooled-reactors-with-increased-accident-tolerance-actof> (accessed 16 november 2022).
- Massey, C.P., Terrani, K.A., Dryepont, S.N., Pint, B.A., 2016. Cladding burst behavior of Fe-based alloys under LOCA. *J. Nucl. Mater.* 470, 128–138. <https://doi.org/10.1016/j.jnucmat.2015.12.018>.
- Nelson, A.G., Martin, N., Kasam-Griffith, A., Xu, Z., Heidet, F., 2022. Uncertainty Quantification Approach for the Versatile Test Reactor Core Design. *Nucl. Sci. Eng.* 196 (sup1), 63–70. <https://doi.org/10.1080/00295639.2022.2035181>.
- Taylor, J.R., 2012. An Introduction to Error Analysis: The Study of Uncertainties in Physical Measurements, second ed. University Science Books, Sausalito <https://isbnsearch.org/isbn/9780935702422>.
- Terrani, K.A., Zinkle, S.J., Snead, L.L., 2014. Advanced oxidation-resistant iron-based alloys for LWR fuel cladding. *J. Nucl. Mater.* 448, 20–435. <https://doi.org/10.1016/j.jnucmat.2013.06.041>.
- Tunes, M.A., Greaves, G., Kremmer, T.M., Vishnyakov, V.M., Edmondson, P.D., Donnelly, S.E., Pogatscher, S., Schön, C.G., 2019. Thermodynamics of an austenitic stainless steel (AISI-348) under in situ TEM heavy ion irradiation. *Acta Mater.* 179, 360–371. <https://doi.org/10.1016/j.actamat.2019.08.041>.
- Urbanic, V.F., Heidrick, T.R., 1978. High-temperature oxidation of Zircaloy-2 and Zircaloy-4 in steam. *J. Nucl. Mater.* 75, 251–261. [https://doi.org/10.1016/0022-3115\(78\)90006-5](https://doi.org/10.1016/0022-3115(78)90006-5).
- USNRC., 2007a. Standard Review Plan (NUREG-0800). 15.0.2 Review of Transient and Accident Analysis Methods <https://www.nrc.gov/docs/ML0708/ML070820123.pdf> (accessed 17 august 2022).
- USNRC., 2007b. Standard Review Plan (NUREG-0800). 4.2 Fuel System Design <https://www.nrc.gov/docs/ML0707/ML070740002.pdf> (accessed 18 august 2022).
- USNRC., 2021a. § 50.46 Acceptance criteria for emergency core cooling systems for light-water nuclear power reactors <https://www.nrc.gov/reading-rm/doc-collections/cfr/part050/part050-0046.html> (accessed 17 august 2022).
- USNRC., 2021b. Appendix K to Part 50—ECCS Evaluation Models <https://www.nrc.gov/reading-rm/doc-collections/cfr/part050/part050-appk.html> (accessed 16 august 2022).